



# Applied Catalysis B: Environmental

journal homepage: [www.elsevier.com/locate/apcatb](http://www.elsevier.com/locate/apcatb)

## Research paper

# Insights into oxygen reduction reaction (ORR) and oxygen evolution reaction (OER) active sites for nitrogen-doped carbon nanostructures ( $CN_x$ ) in acidic media



Kuldeep Mamtani<sup>a</sup>, Deeksha Jain<sup>a</sup>, Doruk Dogu<sup>a</sup>, Vance Gustin<sup>a</sup>, Seval Gunduz<sup>a</sup>, Anne C. Co<sup>b</sup>, Umit S. Ozkan<sup>a,\*</sup>

<sup>a</sup> William G. Lowrie Department of Chemical and Biomolecular Engineering, The Ohio State University, Columbus OH 43210, USA

<sup>b</sup> Department of Chemistry and Biochemistry, The Ohio State University, Columbus OH 43210, USA

## ARTICLE INFO

### Article history:

Received 16 January 2017

Received in revised form 2 June 2017

Accepted 28 July 2017

Available online 5 August 2017

### Keywords:

ORR

OER

$CN_x$

Active sites

Regenerative fuel cells

## ABSTRACT

This study demonstrates promising bifunctionality of nitrogen-doped carbon nanostructures ( $CN_x$ ) for ORR and OER in acidic medium. Although  $CN_x$  catalysts are not as active as Pt/C in ORR and Ir/C in OER, they exhibit significantly lower combined overpotential for ORR and OER relative to those shown by the two commercial catalysts, which are highly active only for one of the two reactions, but not both. The effect of various nitrogen functionalities on the ORR and OER activity of  $CN_x$  catalysts was also studied.  $CN_x$  samples with higher pyridinic-N site density exhibited higher ORR and OER activity.

© 2017 Elsevier B.V. All rights reserved.

## 1. Introduction

Oxygen reduction reaction (ORR) and oxygen evolution reaction (OER) are becoming increasingly important electrochemical reactions due to growing emphasis on sustainable power generation technologies [1,2]. An example of this class of technologies is a proton exchange membrane (PEM) fuel cell where hydrogen (fuel) is oxidized at the anode producing protons which are transported through the electrolyte (membrane) to the cathode where oxygen is reduced forming water. The low temperature of operation (<80 °C) and slow kinetics of hydrogen oxidation and particularly oxygen reduction necessitate Pt-based electrocatalysts [3,4]. Similarly, oxygen evolution reaction (OER), relevant from the point of water electrolysis employs ruthenium or iridium-based catalysts [5,6]. Thus, both reactions use precious metal-based electrocatalysts which are expensive and available only in limited reserves making a strong case to develop low-cost, active and stable electrocatalysts for the two reactions. Furthermore, bifunctionality for ORR and OER is important and extremely relevant for regenerative fuel cell systems. Nitrogen-doped carbon nanostructures or " $CN_x$ "

are considered as promising alternatives [7–15]. As an example,  $CN_x$  materials can be synthesized using chemical vapor deposition of a C and N source (such as CH<sub>3</sub>CN) over a metal-doped support (such as MgO, SiO<sub>2</sub>, or Al<sub>2</sub>O<sub>3</sub>) followed by an acid-washing step to remove the exposed metal and the oxide support [16,17]. Thus, the metal merely acts to initiate growth of  $CN_x$ , and is not accessible on the surface where electrocatalysis occurs. Though these  $CN_x$  materials have been shown to exhibit both ORR and OER activity, the nature of their active sites still remains disputed. There are contradicting reports in the literature suggesting the role of various nitrogen species in imparting catalytic activity to these materials [7,10–13,18–27]. Though techniques such as Mössbauer spectroscopy or X-ray Absorption Spectroscopy (XAS) are widely used to reveal active sites and compute their density for metal-centered catalysts [28,29], they are of little use in the case of  $CN_x$  due to the absence of a metal-center. In-addition, absence of poisoning using well-known probes such as CO, CN<sup>−</sup> and H<sub>2</sub>S [10,15,30,31] makes identification and quantification of active sites in these materials even more challenging.

With this motivation, we have recently focused on devising strategies that can help reveal the active sites in  $CN_x$  materials. One of these is related to identification of a probe molecule which poisons these  $CN_x$  catalysts and thus provides insights about their active sites [32]. We recently demonstrated, for the first time,

\* Corresponding author.

E-mail address: ozkan.1@osu.edu (U.S. Ozkan).

that ORR active sites in CN<sub>x</sub> catalysts can be probed using phosphate anion poisoning. The loss in pyridinic-N site density was observed to be correlated to the loss in ORR activity. Based on these results, we hypothesized two possible active site models namely i) pyridinic-N sites and ii) C atoms next to pyridinic-N. The former would be rendered inactive by protonation whereas the latter by a site blocking effect of the phosphate ions which would also stabilize the pyridinic-NH sites [32]. Another useful approach is to modify the pyrolysis conditions such that the amount of various nitrogen species on the surface can be controlled. This latter approach is also the focus of this work. The first part of the study aims to evaluate the bifunctional characteristics of these CN<sub>x</sub> catalysts for ORR and OER. Comparisons with the state-of-the-art catalyst materials for ORR and OER are also presented. In the second part of the study, CN<sub>x</sub> catalysts were synthesized using different pyrolysis temperatures, but the same C, N source. This allowed us to control the distribution of various nitrogen functionalities in the synthesized materials. ORR and OER activities of these samples were then correlated to the amount of each of these nitrogen species. Results from characterization experiments using X-ray Photoelectron Spectroscopy (XPS) and Laser Raman Spectroscopy (LRS) are also presented.

## 2. Experimental

### 2.1. Materials

The growth substrates for the CN<sub>x</sub> catalysts were prepared through incipient wet impregnation technique on MgO (Aldrich) support by using 2 wt% iron (from iron (II) acetate, Aldrich) dissolved in deionized water, the volume of which was decided based on the pore volume of the support. The sample was then kept overnight in an oven for solvent evaporation and then ball-milled at 200 rpm for 3 h using a rotary ball-mill. The ball-milled substrate then went through an acetonitrile pyrolysis step for 2 h at 900 °C for the carbon growth process. The resulting sample was then subjected to an acid-washing step in 1 M HCl for 1 h at 60 °C and then vacuum-filtered, washed and dried in an oven at 80 °C. The final product collected from the oven is denoted as CN<sub>x</sub>. Similarly, CN<sub>x</sub> was also synthesized using pyrolysis temperatures of 750 °C, 800 °C and 850 °C respectively. 10% Pt/C (ETEK) and 20% Ir/C (Premetek Co.) were used as received as the state-of-the-art catalyst materials for ORR and OER, respectively.

### 2.2. Electrochemical testing

Oxygen reduction reaction (ORR) activity was measured in a standard three-electrode system comprising of a working electrode (glassy carbon disk, 5.61 mm and 0.2472 cm<sup>2</sup>), a hydrogen reference electrode (ET070 Hydroflex) and a counter electrode (Pt coil). The electrolyte used was 0.1 M HClO<sub>4</sub>. To prepare the CN<sub>x</sub> catalyst ink, 95 µL of 5 wt% Nafion® solution and 350 µL ethanol (200 proof) were added to 10 mg of catalyst weighed in a 2 mL vial. The vial was then kept for ultrasonication in an ice bath until the catalyst was well-dispersed. A 9 µL aliquot of the ink was then pipetted onto the glassy carbon disk which corresponded to a catalyst loading of about 800 µg/cm<sup>2</sup> geometric.

The catalyst ink preparation procedure was similar for Pt/C and Ir/C and the catalyst loading (including the mass of carbon) was about 200 µg/cm<sup>2</sup> geometric for these samples.

Cyclic voltammograms (CVs) were first collected at 50 mV/s from 1.2 V to 0 V to 1.2 V with the working electrode rotating at 1000 rpm until reproducible CVs were noted in the oxygen saturated electrolyte. Slow CVs at 10 mV/s were then collected at 400, 800, 1000, 1200 and 1600 rpm on the disk again from 1.2 V to 0 V

to 1.2 V. CVs were also collected in an argon saturated electrolyte serving as a blank.

ORR performance was evaluated by comparing (i) potential at a background-subtracted current density of -0.1 mA/cm<sup>2</sup>, (ii) half-wave potential (E<sub>1/2</sub>), (iii) specific kinetic current (i<sub>K</sub>) at 0.7 V. Calculation of specific kinetic current for ORR was made using the Koutechy-Levich equation Eq. (1).

$$\frac{1}{i} = \frac{1}{i_K} + \frac{1}{i_{lim}} \quad (1)$$

where i is the measured current density,

i<sub>K</sub> is the kinetic current density defined by  $i_K = nFkC_{O_2}$   
and i<sub>lim</sub> is the limiting current density defined by  $i_{lim} = 0.62nFD^{2/3}C_{O_2}\vartheta^{-1/6}$ .

Here, n is the number of electrons transferred per molecule of oxygen, F is the Faraday's constant (96485 C/mole of electrons), k is the rate constant for ORR, C<sub>O<sub>2</sub></sub> is the bulk concentration of oxygen ( $1.18 \times 10^{-6}$  mol/cm<sup>3</sup>) [33,34], D is the diffusion coefficient of oxygen ( $1.93 \times 10^{-5}$  cm<sup>2</sup>/s) [33–35], θ is the kinematic viscosity of the electrolyte ( $1.009 \times 10^{-2}$  cm<sup>2</sup>/s) [33,35].

In-addition, Tafel analysis was performed to gain insights into the rate-determining step for ORR using Eq. (2).

$$V = V_0 + b \log \frac{i}{i_0} \quad (2)$$

where V<sub>0</sub> is the equilibrium potential (1.23 V), b is the Tafel slope and i<sub>0</sub> is the exchange current density.

To evaluate OER activity, linear sweep voltammograms (LSVs) were collected from 0.0 to 2.0 V in an argon-saturated electrolyte with the catalyst-coated electrode rotating at 1600 rpm. The scan rate used was 10 mV/s. The capacitive current was subtracted from the measured total OER current. The current observed below 1.3 V was assumed as the capacitive contribution and was consequently subtracted from the overall measured current. Potential at an OER current density (after subtracting the capacitive component) of 10 mA/cm<sup>2</sup> geometric was considered as a measure of OER activity.

All potentials referred to in this work are referenced with respect to a reversible hydrogen electrode (RHE) scale.

### 2.3. Characterization

X-ray Photoelectron Spectroscopy (XPS) was used to analyze the composition of the surface species. A Kratos Axis Ultra DLD Spectrometer was used with Al K $\alpha$  monochromatic X-ray radiation (1486.6 eV). The spectra were collected at room temperature with 20 eV pass energy. Binding energy (B.E.) values were referenced to the standard C 1s binding energy of 284.5 eV. CasaXPS program was used for data analysis and curve fitting. Shirley-type background and Lorentzian-Gaussian combination were used for data processing.

Laser Raman Spectroscopy experiments were performed at room temperature using a LabRAM HR Raman microscope system from Horiba Scientific. All measurements were performed at room temperature using 514.5 nm laser and a 50x objective. Before collecting the spectra, calibration was made using a silicon reference at 520.7 cm<sup>-1</sup> and white light at 0 cm<sup>-1</sup>. The spectrograph uses a grating of 1200 lines/mm. Multiple spectra were collected and averaged to improve the signal to noise ratio. The peak assignments were based on the literature. Data analysis and curve fitting were performed using MagicPlot program.

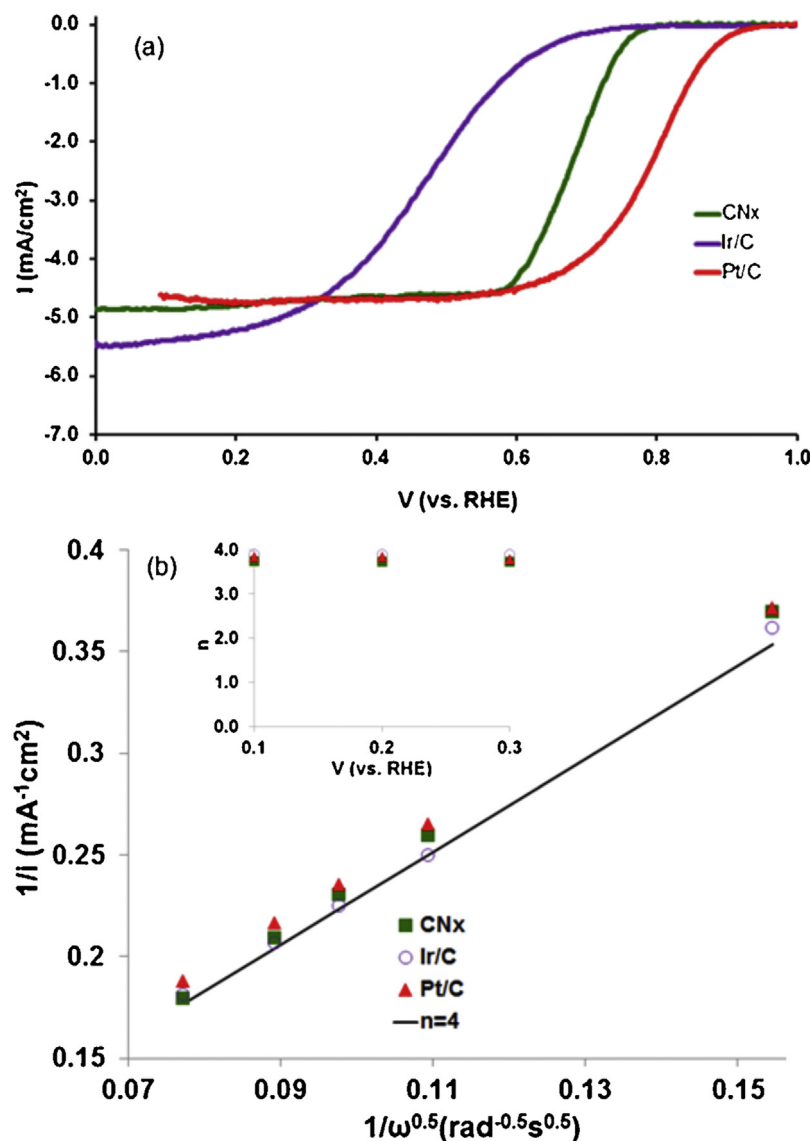


**Fig. 1.** Polarization curves (a) and Koutechy-Levich plots (b) at 0.2 V vs. RHE of CN<sub>x</sub>, Ir/C and Pt/C samples for ORR. The theoretical line corresponding to selectivity (n) of 4 is also included in (b). Inset in (b) represents selectivity (n) as a function of potential (V) for various samples. (O<sub>2</sub> saturated, 0.1 M HClO<sub>4</sub>, 1600 rpm, 10 mV/s and 800 μg<sub>catalyst</sub>/cm<sup>2</sup> geometric).

### 3. Results and discussion

#### 3.1. Bifunctional characteristics of CN<sub>x</sub>

The ORR activity for CN<sub>x</sub> catalyst as well as that for commercial Ir/C and Pt/C samples was measured. As seen in Fig. 1(a), Ir/C exhibited the lowest ORR activity whereas Pt/C showed the highest ORR activity. The ORR activity for CN<sub>x</sub> catalyst was found to be higher than Ir/C, but lower than that for Pt/C sample. However, it should be noted that the onset potential and half-wave potential

**Table 1**  
Comparison of ORR kinetic parameters for various samples

Sample	V vs. RHE @ -0.1 mA/cm <sup>2</sup> geometric	Half-wave potential E <sub>1/2</sub> (V vs. RHE)
Ir/C	0.72	0.47
Pt/C	0.92	0.79
CN <sub>x</sub>	0.78	0.68

(E<sub>1/2</sub>) values for the CN<sub>x</sub> catalyst were lower than those for Pt/C by only 140 mV and 110 mV, respectively (Table 1). This demon-

**Table 2**  
Inspection of catalyst bifunctional activity of various samples.

Sample	Measure of ORR activity V vs. RHE @ -3 mA/cm <sup>2</sup> geometric	Measure of OER activity V vs. RHE @ 10 mA/cm <sup>2</sup> geometric	Measure of bifunctional catalytic activity (Total overpotential requirement for ORR and OER) Δ V (OER-ORR)
Ir/C	0.45	1.59	1.14
Pt/C	0.76	1.87	1.11
CN <sub>x</sub>	0.66	1.62	0.96

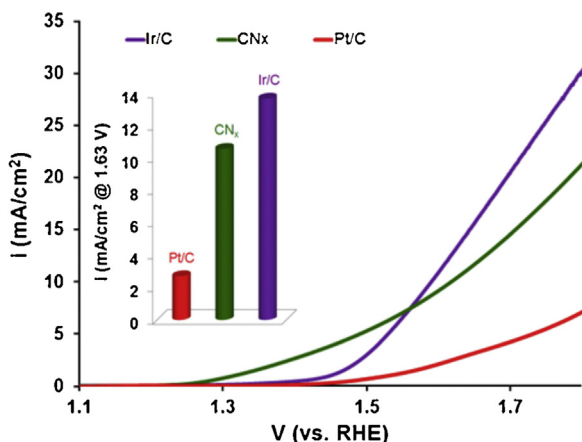


**Fig. 2.** Linear sweep voltammograms of CN<sub>x</sub>, Ir/C and Pt/C samples for OER. (Ar saturated, 0.1 M HClO<sub>4</sub>, 1600 rpm, 10 mV/s and 800  $\mu\text{g}_{\text{catalyst}}/\text{cm}^2$  geometric). Inset represents OER current at 1.63 V vs. RHE for all samples.

strates significant ORR activity of CN<sub>x</sub> materials. On the other hand, Ir/C sample showed significantly lower onset potential (0.72 V) and  $E_{1/2}$  (0.47 V) compared to Pt/C and CN<sub>x</sub> catalysts.

We also measured the selectivity of these catalysts towards water formation. Fig. 1(b) presents the corresponding Koutechy-Levich plots at 0.2 V for Ir/C, Pt/C and CN<sub>x</sub> samples. The plots were found to be linear and parallel for all three samples. The slope of these plots were used to obtain selectivity (*n*) which was found to be close to 4 for all catalysts tested, suggesting that oxygen is primarily reduced via a four-electron pathway (either as direct 4e<sup>-</sup> reduction to H<sub>2</sub>O or a two-step reduction to a H<sub>2</sub>O<sub>2</sub> intermediate, then to H<sub>2</sub>O, with 2e<sup>-</sup> involved in each step). The selectivity values for all these samples were found to be weakly dependent on the potential as represented in the inset of Fig. 1(b).

The anodic linear sweep voltammograms (LSVs) were collected in argon-saturated 0.1 M HClO<sub>4</sub> for Ir/C, Pt/C and CN<sub>x</sub> samples to measure the OER activity. The OER currents for these samples after subtracting the capacitive component from the overall measured current are shown in Fig. 2. Among the three samples investigated here, Pt/C exhibited the lowest OER activity as indicated by its significantly higher overpotential requirements. On the other hand, the potential at a current density of 10 mA/cm<sup>2</sup> geometric, considered here as a measure of OER activity [36], was found to be similar for CN<sub>x</sub> sample compared to that for a state-of-the-art catalyst for OER namely Ir/C (1.62 V vs. 1.59 V). The OER currents at 1.63 V for CN<sub>x</sub> were about 77% of the current for Ir/C as noted in the inset of

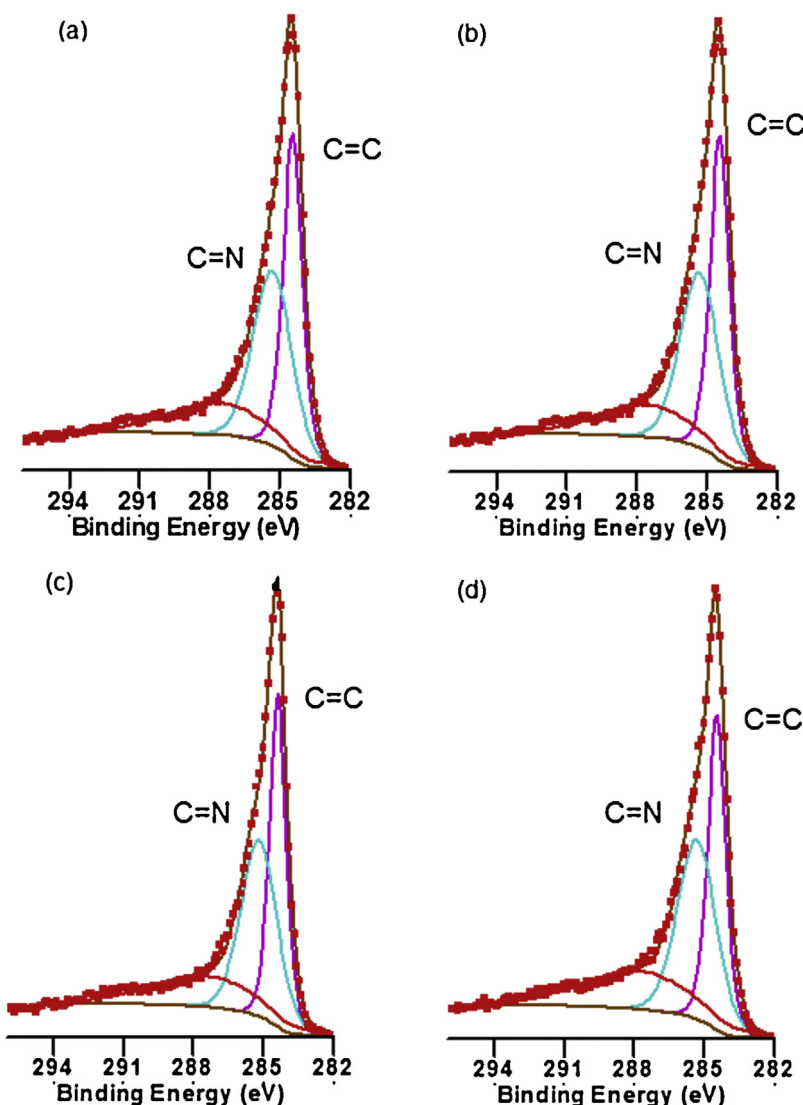


**Fig. 3.** C 1s XPS spectra for samples pyrolyzed at various temperatures. (a): 750 °C, (b): 800 °C, (c): 850 °C and (d): 900 °C.

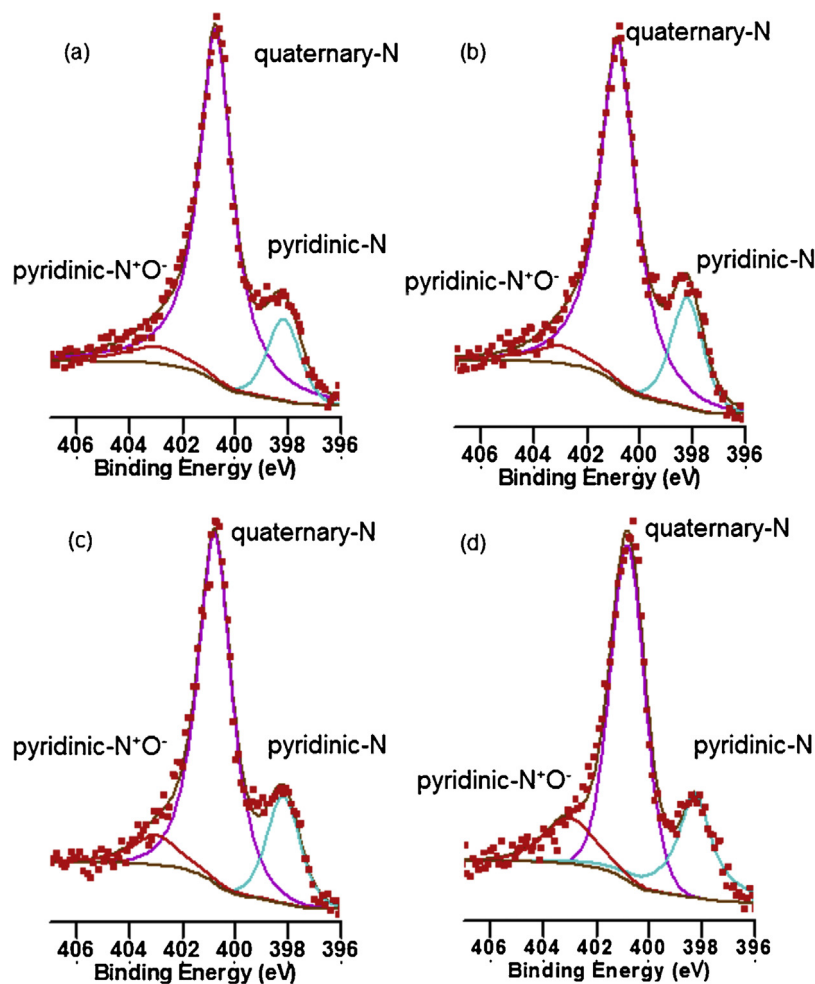


**Fig. 4.** N 1s XPS spectra for samples pyrolyzed at various temperatures. (a): 750 °C, (b): 800 °C, (c): 850 °C and (d): 900 °C.

**Fig. 2.** This is a very significant result from a practical viewpoint if we consider the enormous difference in the cost of these catalysts [37].

The bifunctional electrocatalytic activity of the three samples under consideration was next evaluated for ORR and OER. This analysis was performed using the total overpotential requirement of each of these samples for the two reactions. For this, the overpotential at an ORR current density of  $-3 \text{ mA/cm}^2$  ( $\eta_{\text{ORR}}$ ) was added to the overpotential at an OER current density of  $10 \text{ mA/cm}^2$  ( $\eta_{\text{OER}}$ ) [36,38,39]. Table 2 presents the results from this analysis. The total overpotential requirement for Ir/C and Pt/C were found to be similar (1.14 V and 1.11 V). This is quite expected considering the results presented earlier. It was noted that Ir/C has poor ORR activity, but good OER activity whereas Pt/C exhibited excellent ORR activity, but very low OER activity. Thus, each of these catalysts performed well only for one of the two reactions. This is in sharp contrast to CN<sub>x</sub> catalyst materials which demonstrated much better bifunctional characteristics as evident from its significantly lower total overpotential requirements (Table 2).

Stability is an important consideration for ORR and OER on carbon-based materials in acidic media. In our earlier work, we had compared CN<sub>x</sub> catalysts with Vulcan carbon, which is commonly used as a support material for precious metals, and had found these nitrogen-doped carbon materials to be much more resistant to carbon corrosion than Vulcan carbon [40]. Moreover, we have recently reported that nitrogen-coordinated iron carbon (FeNC) catalysts are stable under OER conditions in acidic media [41]. The stability of CN<sub>x</sub> catalysts was also examined under OER conditions. It was

found that the OER current density at various potentials (1.45, 1.5, 1.55, 1.6 and 1.63 V) decreased slightly initially and then remained stable up to 100 cycles (Fig. S1). Furthermore, electrochemically active surface area of CN<sub>x</sub> obtained after 100 cycles was found to be the same as that measured before performing OER, which also provides evidence of stability (Fig. S2).

In order to exclude the possibility of any carbon corrosion, we used a special electrochemical half-cell that can be sealed and connected the effluent gas stream from the cell to a mass spectrometer. The signals for O<sub>2</sub> (32) and CO<sub>2</sub> (44) were monitored before, during and after application of a constant current of  $1 \text{ mA/cm}^2$  to the working electrode. This experiment confirmed that the OER current obtained using CN<sub>x</sub> catalysts was indeed due to evolution of oxygen and not a result of carbon corrosion (Fig. S3). The resistance of CN<sub>x</sub> to carbon corrosion in acidic media can be attributed to its graphitic nature which was confirmed using X-ray diffraction (XRD) analysis as shown in Fig. S4 [42,43].

### 3.2. CN<sub>x</sub> catalysts with different relative distribution of nitrogen species

As discussed in the previous section, CN<sub>x</sub> materials are promising bifunctional electrocatalysts for ORR and OER. However, as also pointed out in the introduction section, the nature of ORR and OER active sites in these materials is not clearly understood. With this objective, we synthesized CN<sub>x</sub> catalysts with different relative dis-

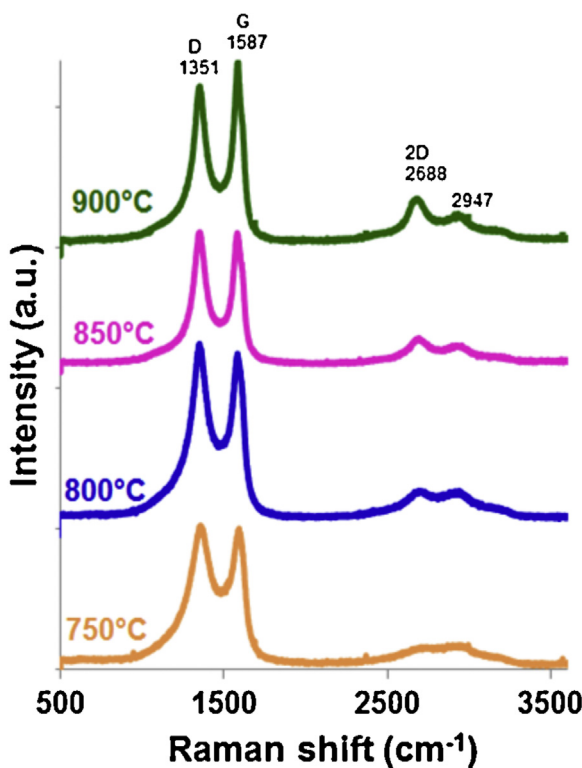


**Fig. 5.** Raman spectra for  $\text{CN}_x$  catalysts synthesized at various temperatures.

tribution of nitrogen species on the surface as discussed in the subsequent sections.

### 3.3. XPS

The nature of the surface species on various  $\text{CN}_x$  samples pyrolyzed at various temperatures was studied using XPS. The sur-

**Table 3**  
Surface elemental composition for samples pyrolyzed at various temperatures as determined by XPS.

Pyrolysis Temperature (°C)	Atomic%		
	C	N	O
900	90	7	3
850	91	7	2
800	91	7	2
750	90	7	3

face elemental composition confirms that there is a significant amount of carbon with no Fe present on the surface of all samples, the other elements on the surface being nitrogen and oxygen (Table 3). It is important to note that the total nitrogen content and consequently the C:N ratio is the same on all samples. This is expected considering the fact that the same C, N source was used for synthesizing all samples.

The C 1s spectra for  $\text{CN}_x$  samples synthesized using various pyrolysis temperatures are presented in Fig. 3. The presence of  $\text{C}=\text{C}$  (B.E. of 284.4–284.5 eV) [21] and  $\text{C}=\text{N}$  bonds (B.E. of 285.2–285.3 eV) [21] was confirmed in all samples. The higher binding energy peak also observed in all samples is attributed to oxidized carbon species such as  $\text{O}=\text{C}$  or  $\text{O}—\text{C}=\text{O}$  [44,45].

Fig. 4 compares the corresponding N 1s XPS spectra for various  $\text{CN}_x$  samples. All samples exhibited three types of nitrogen functionalities namely pyridinic-N (398.2 – 398.3 eV) [46,47], quaternary-N (400.7–400.8 eV) [12] and pyridinic- $\text{N}^+ \text{O}^-$  ( $>402$  eV) [48]. However, the relative distribution of these nitrogen species was different as seen in Table 4.

### 3.4. Laser Raman Spectroscopy

The Raman spectra for various  $\text{CN}_x$  samples are shown in Fig. 5. The results from the deconvolution of these spectra [49–51] are presented in Fig. 6. All samples exhibited the presence of first-order D and G bands centered at 1351 and 1589  $\text{cm}^{-1}$  (mean values) [50,51]. The D band arises due to disorder and corresponds to carbon atoms

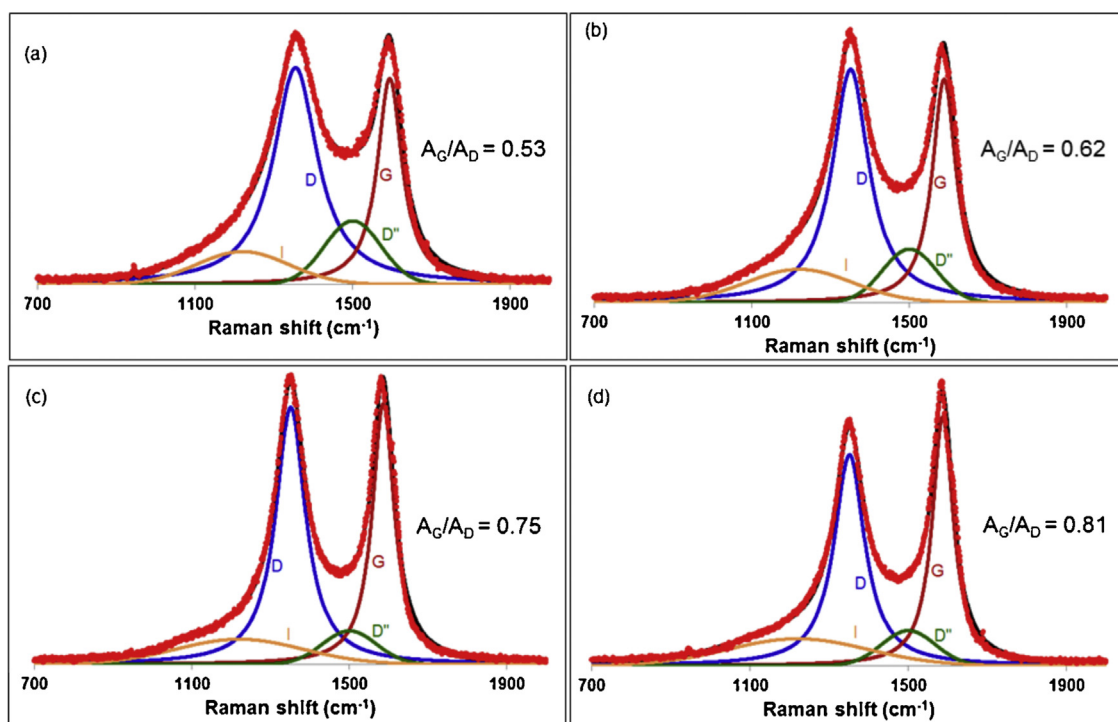


**Fig. 6.** Deconvoluted Raman spectra for  $\text{CN}_x$  catalysts synthesized at various temperatures. (a): 750 °C, (b): 800 °C, (c): 850 °C and (d): 900 °C.

**Table 4**

N 1s distribution for samples pyrolyzed at various temperatures as determined by XPS.

Pyrolysis Temperature (°C)	Relative% distribution		
	pyridinic-N (398.2–398.3 eV)	quaternary-N (400.7–400.8 eV)	pyridinic-N <sup>+</sup> O <sup>-</sup> (>402 eV)
900	26	61	13
850	20	72	8
800	18	75	7
750	14	80	6

near the edges of a graphene layer. The G band is attributed to the presence of graphitic carbon and associated with an ideal graphitic lattice vibration mode. The ratio of the area of D band to that of G band corresponds to the density of defects in the lattice. Similarly, the ratio of the area of G band to that of D band corresponds to the degree of crystallinity or graphitization in the sample of interest. It is noted from Fig. 6 that the degree of graphitization ( $A_{G\text{band}}/A_{D\text{band}}$ ) somewhat increased with increasing pyrolysis temperature. In addition to the D and G bands, presence of bands at Raman shifts of  $1220\text{ cm}^{-1}$  and  $1500\text{ cm}^{-1}$  was also confirmed for all samples, based on the fit to the spectra. These are referred to as I and D" bands. I band has also been associated with C=C stretching vibrations or ionic impurities [50,52]. On the other hand, D" band corresponds to amorphous carbon [50,52] which generally decreases with increasing pyrolysis temperature. It is interesting to note that bands at higher Raman shift ( $>2000\text{ cm}^{-1}$ ) were prominent only for samples pyrolyzed at higher temperatures (Fig. 5).

### 3.5. Electrochemical testing

The ORR and OER activities of  $\text{CN}_x$  samples synthesized using various pyrolysis temperatures were measured from the cathodic polarization curves shown in Fig. 7(a).

The mass-transport corrected Tafel plots in Fig. 7(b) were obtained using the corresponding polarization curves and specific kinetic current ( $i_K$ ) values from Koutechy-Levich equation (equation I). It is evident from Fig. 7(a) and (b) that ORR activity increased as the pyrolysis temperature increased from  $750\text{ }^\circ\text{C}$  to  $900\text{ }^\circ\text{C}$ . Comparison of the ORR kinetic parameters for various  $\text{CN}_x$  samples is also presented in Table 5.

Fig. 7(c) presents the Koutechy-Levich plots at  $0.1\text{ V}$ . The plots were found to be linear and parallel at potentials in the range of  $0.1\text{--}0.3\text{ V}$ .

The selectivity ( $n$ ) was found to be around 4 for all samples except the one pyrolyzed at  $750\text{ }^\circ\text{C}$ . This observation suggests that pyrolysis temperatures of  $800\text{ }^\circ\text{C}$  and above facilitate  $\text{O}_2$  reduction via an overall four-electron transfer to  $\text{H}_2\text{O}$ . The potential did not affect the selectivity significantly for any sample as seen in the inset of Fig. 7(c).

The OER voltammograms for various  $\text{CN}_x$  samples are shown in Fig. 8. The potential value at an OER current density of  $10\text{ mA}/\text{cm}^2$  and considered as a measure of OER activity is compared for various  $\text{CN}_x$  samples in Table 6. It is evident that OER activity was lowest for  $750\text{ }^\circ\text{C}$  and highest for  $900\text{ }^\circ\text{C}$  (Table 6).

**Table 5**

Comparison of ORR kinetic parameters for various samples.

Pyrolysis Temperature (°C)	V vs. RHE @ $-0.1\text{ mA}/\text{cm}^2$ geometric	Half-wave potential $E_{1/2}$ (V vs. RHE)	$i_K$ ( $\text{mA}/\text{mg}_{\text{catalyst}}$ ) @ $0.7\text{ V}$ vs. RHE
900	0.78	0.68	3.24
850	0.76	0.65	1.55
800	0.75	0.57	0.55
750	0.70	0.50	0.17

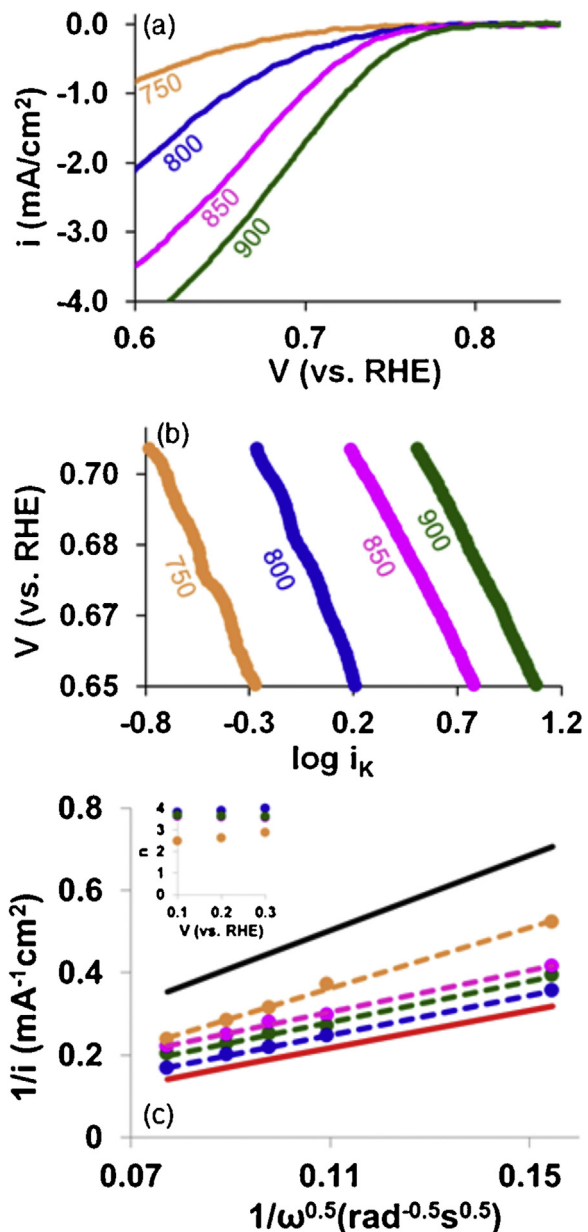
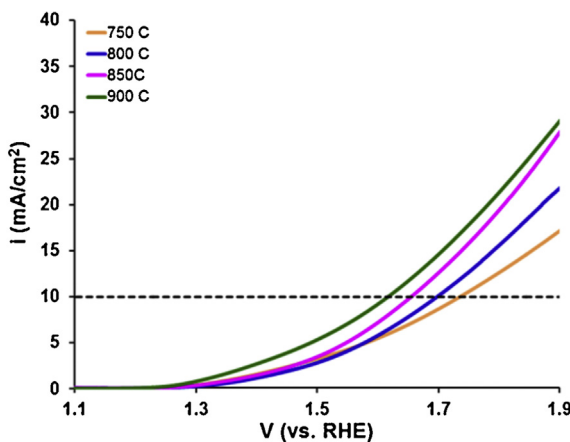


Fig. 7. (a) High potential regions of the cathodic polarization curves and (b) mass transport corrected Tafel plots of samples pyrolyzed at various temperatures for ORR. Koutechy-Levich plots at  $0.1\text{ V}$  vs. RHE are represented in (c). The theoretical lines corresponding to selectivity ( $n$ ) of 2 (solid black) and 4 (solid red) as well as the linear fits (dashed) are also included in (c). Inset in (c) represents selectivity ( $n$ ) as a function of potential ( $V$ ) for various samples. ( $\text{O}_2$  saturated,  $0.1\text{ M HClO}_4$ ,  $1600\text{ rpm}$ ,  $10\text{ mV/s}$  and  $800\text{ }\mu\text{g}_{\text{catalyst}}/\text{cm}^2$  geometric). (For interpretation of the references to colour in this figure legend, the reader is referred to the web version of this article.)



**Fig. 8.** Linear sweep voltammograms for various samples for OER. (Ar saturated, 0.1 M HClO<sub>4</sub>, 1600 rpm, 10 mV/s and 800 µg<sub>catalyst</sub>/cm<sup>2</sup> geometric).

**Table 6**  
Comparison of OER activity for various samples.

Pyrolysis Temperature (°C)	V vs. RHE @ 10 mA/cm <sup>2</sup> geometric)
900	1.62
850	1.66
800	1.70
750	1.74

### 3.6. Effect of various nitrogen species on ORR and OER activity

The ORR and OER activities of various CN<sub>x</sub> samples were next correlated with the amounts of various nitrogen species identified using XPS. Though the total nitrogen content was the same in all CN<sub>x</sub> samples, the relative distribution of various nitrogen species and consequently their site density was different amongst various samples.

When specific kinetic current ( $i_K$ ) at 0.7 V, a typical measure of ORR activity was plotted as a function of relative distribution of various nitrogen species as determined by XPS, it was found that ORR activity did not correlate with the relative distribution of quaternary-N. On the other hand,  $i_K$  correlated very well with the amount of pyridinic-N species (Fig. 9a). Similar trends were observed for OER activity where it was found that potential at 10 mA/cm<sup>2</sup> as well as specific OER current at 1.63 V correlated with the amount of pyridinic-N species (Fig. 9b) but not with that of quaternary-N functionalities. In addition, the combined overpotential for ORR and OER determined from the bifunctionality analysis as discussed before decreased with increasing abundance of pyridinic-N species as represented in Fig. 9c.

Thus, XPS results presented here provide evidence that pyridinic-N species are important in catalyzing the ORR and OER on CN<sub>x</sub> catalyst materials in acidic medium. However, whether pyridinic-N species are themselves the active sites or merely impart Lewis basicity to adjacent C-atoms and thereby making them ORR and OER active needs further investigation. It should be noted that pyridinic-N<sup>+</sup>O<sup>-</sup> species were not considered for discussion here because they are most likely formed as a result of oxidation of pyridinic-N species [7,48,53,54].

## 4. Conclusions

The present study demonstrates the promise of CN<sub>x</sub> catalyst materials for regenerative fuel cell systems. Evaluation of bifunctional characteristics suggests significantly lower combined ORR and OER overpotential for these catalysts compared to Pt/C and Ir/C. In-addition, CN<sub>x</sub> catalysts were synthesized with varied rela-

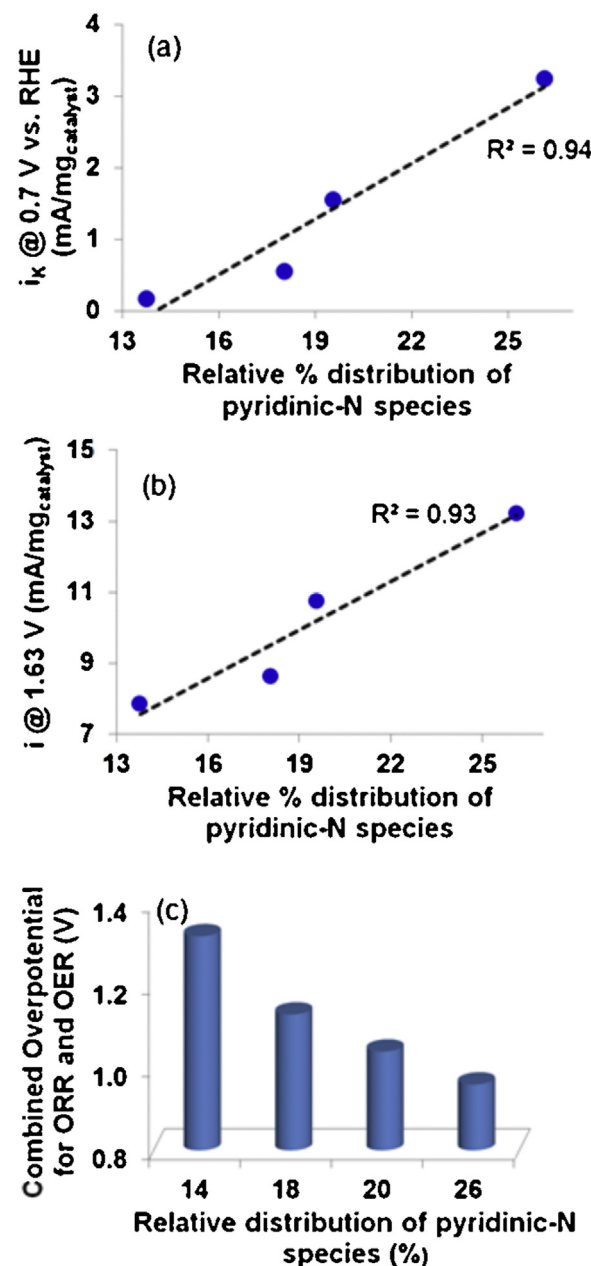


**Fig. 9.** Correlation of pyridinic nitrogen content to (a) ORR activity, (b) OER activity and (c) combined overpotential for ORR and OER of CN<sub>x</sub> catalysts synthesized at various temperatures.

tive distribution of various nitrogen functionalities on the surface. The ORR and OER activity was observed to increase with increase in pyridinic-N site density. Also, rapid cycling experiments and monitoring the half-cell effluent by a mass spectrometer showed these catalysts to be stable and ruled out the possibility of any carbon corrosion. We believe that the insights gained from this study will be useful for rational catalyst design.

## Acknowledgements

This material is based upon work supported by the U.S. Department of Energy, Office of Science, Office of Basic Energy Sciences under Award Number DE-FG02-07ER15896. We would also like to thank Ohio Coal Research Consortium for their financial support under Subcontract No. OCRC-C-04.

## Appendix A. Supplementary data

Supplementary data associated with this article can be found, in the online version, at <http://dx.doi.org/10.1016/j.apcatb.2017.07.086>.

## References

- [1] S. Chu, A. Majumdar, Opportunities and challenges for a sustainable energy future, *Nature* 488 (2012) 294–303.
- [2] S. Gupta, W. Kellogg, H. Xu, X. Liu, J. Cho, G. Wu, Bifunctional perovskite oxide catalysts for oxygen reduction and evolution in alkaline media, *Chem. Asian J.* 11 (2016) 10–21.
- [3] S. Mukerjee, S. Srinivasan, M.P. Soriaga, Role of structural and electronic properties of pt and Pt alloys on electrocatalysis of oxygen reduction, *J. Electrochem. Soc.* 142 (1995) 1409–1422.
- [4] H.A. Gasteiger, S.S. Kocha, B. Sompalli, F.T. Wagner, Review – activity benchmarks and requirements for Pt, Pt-alloy, and non-Pt oxygen reduction catalysts for PEMFCs, *Appl. Catal. B-Environ.* 56 (2005) 9–35.
- [5] Y. Zhao, E.A. Hernandez-Pagan, N.M. Vargas-Barbosa, J.L. Dysart, T.E. Mallouk, A high yield synthesis of ligand-free iridium oxide nanoparticles with high electrocatalytic activity, *J. Phys. Chem Lett.* 2 (2011) 402–406.
- [6] T. Nakagawa, C.A. Beasley, R.W. Murray, Efficient electro-Oxidation of water near its reversible potential by a mesoporous IrO<sub>x</sub> nanoparticle film, *J. Phys. Chem. C* 113 (2009) 12958–12961.
- [7] P.H. Matter, L. Zhang, U.S. Ozkan, The role of nanostructure in nitrogen-containing carbon catalysts for the oxygen reduction reaction, *J. Catal.* 239 (2006) 83–96.
- [8] K. Mamanti, U.S. Ozkan, Heteroatom-doped carbon nanostructures as oxygen reduction reaction catalysts in acidic media: an overview, *Catal. Lett.* 145 (2015) 436–450.
- [9] R.M. Yadav, J. Wu, R. Kochandra, L. Ma, C.S. Tiwary, L. Ge, G. Ye, R. Vajtai, J. Lou, P.M. Ajayan, Carbon nitrogen nanotubes as efficient bifunctional electrocatalysts for oxygen reduction and evolution reactions, *ACS Appl. Mater. Interfaces* 7 (2015) 11991–12000.
- [10] K. Gong, F. Du, Z. Xia, M. Durstock, L. Dai, Nitrogen-doped carbon nanotube arrays with high electrocatalytic activity for oxygen reduction, *Science* 323 (2009) 760–764.
- [11] X. Li, G. Liu, B.N. Popov, Activity and stability of non-precious metal catalysts for oxygen reduction in acid and alkaline electrolytes, *J. Power Sources* 195 (2010) 6373–6378.
- [12] G. Liu, X. Li, P. Ganesan, B.N. Popov, Studies of oxygen reduction reaction active sites and stability of nitrogen-modified carbon composite catalysts for PEM fuel cells, *Electrochim. Acta* 55 (2010) 2853–2858.
- [13] N.P. Subramanian, X. Li, V. Nallathambi, S.P. Kumaraguru, H. Colon-Mercado, G. Wu, J.-W. Lee, B.N. Popov, Nitrogen-modified carbon-based catalysts for oxygen reduction reaction in polymer electrolyte membrane fuel cells, *J. Power Sources* 188 (2009) 38–44.
- [14] Y. Zhao, R. Nakamura, K. Kamiya, S. Nakanishi, K. Hashimoto, Nitrogen-doped carbon nanomaterials as non-metal electrocatalysts for water oxidation, *Nat. Commun.* 4 (2013) 2390.
- [15] S. Maldonado, K.J. Stevenson, Influence of nitrogen doping on oxygen reduction electrocatalysis at carbon nanofiber electrodes, *J. Phys. Chem. B* 109 (2005) 4707–4716.
- [16] P.H. Matter, E. Wang, U.S. Ozkan, Preparation of nanostructured nitrogen-containing carbon catalysts for the oxygen reduction reaction from SiO<sub>2</sub> and MgO supported metal particles, *J. Catal.* 243 (2006) 395–403.
- [17] P.H. Matter, E. Wang, M. Arias, E.J. Biddinger, U.S. Ozkan, Oxygen reduction reaction catalysts prepared from acetonitrile pyrolysis over alumina supported metal particles, *J. Phys. Chem. B* 110 (2006) 18374–18384.
- [18] S. Kundu, T.C. Nagaiah, W. Xia, Y. Wang, S. Van Dommelle, J.H. Bitter, M. Santa, G. Grundmeier, M. Bron, W. Schuhmann, M. Muhler, Electrocatalytic activity and stability of nitrogen-containing carbon nanotubes in the oxygen reduction reaction, *J. Phys. Chem. C* 113 (2009) 14302–14310.
- [19] C.V. Rao, C.R. Cabrera, Y. Ishikawa, In search of the active site in nitrogen-doped carbon nanotube electrodes for the oxygen reduction reaction, *J. Phys. Chem. Lett.* 1 (2010) 2622–2627.
- [20] V. Nallathambi, J.-W. Lee, S.P. Kumaraguru, G. Wu, B.N. Popov, Development of high performance carbon composite catalyst for oxygen reduction reaction in PEM proton exchange membrane fuel cells, *J. Power Sources* 183 (2008) 34–42.
- [21] J. Wu, L. Ma, R.M. Yadav, Y. Yang, X. Zhang, R. Vajtai, J. Lou, P.M. Ajayan, Nitrogen-doped graphene with pyridinic dominance as a highly active and stable electrocatalyst for oxygen reduction, *ACS Appl. Mater. Interfaces* 7 (2015) 14763–14769.
- [22] D. Guo, R. Shibuya, C. Akiba, S. Saji, T. Kondo, J. Nakamura, Active sites of nitrogen-doped carbon materials for oxygen reduction reaction clarified using model catalysts, *Science* 351 (2016) 361–365.
- [23] A. Dorjgotov, J. Ok, Y. Jeon, S.-H. Yoon, Y.G. Shul, Activity and active sites of nitrogen-doped carbon nanotubes for oxygen reduction reaction, *J. Appl. Electrochem.* 43 (2013) 387–397.
- [24] T. Nagaiah, S. Kundu, M. Bron, M. Muhler, W. Schuhmann, Nitrogen-doped carbon nanotubes as a cathode catalyst for the oxygen reduction reaction in alkaline medium, *Electrochim. Commun.* 12 (2010) 338–341.
- [25] T. Sharifi, G. Hu, X.E. Jia, T. Wagberg, Formation of active sites for oxygen reduction reactions by transformation of nitrogen functionalities in nitrogen-Doped carbon nanotubes, *ACS Nano* 6 (2012) 8904–8912.
- [26] W. Xia, J. Masa, M. Bron, W. Schuhmann, M. Muhler, Highly active metal-free nitrogen-containing carbon catalysts for oxygen reduction synthesized by thermal treatment of polypyridine-carbon black mixtures, *Electrochim. Commun.* 13 (2011) 593–596.
- [27] Y. Qiu, J. Yu, T. Shi, X. Zhou, X. Bai, J.Y. Huang, Nitrogen-doped ultrathin carbon nanofibers derived from electrospinning: large-scale production, unique structure, and application as electrocatalysts for oxygen reduction, *J. Power Sources* 196 (2011) 9862–9867.
- [28] U.I. Kramm, J. Herranz, N. Larouche, T.M. Arruda, M. Lefevre, F. Jaouen, P. Bogdanoff, S. Fiechter, I. Abs-Wurmback, S. Mukerjee, J.P. Dodelet, Structure of the catalytic sites in Fe/N/C-catalysts for O-2-reduction in PEM fuel cells, *Phys. Chem. Chem. Phys.* 14 (2012) 11673–11688.
- [29] U.I. Koslowski, I. Abs-Wurmback, S. Fiechter, P. Bogdanoff, Nature of the catalytic centers of porphyrin-based electrocatalysts for the ORR: a correlation of kinetic current density with site density of Fe-N<sub>4</sub> centers, *J. Phys. Chem. C* 112 (2008) 15356–15366.
- [30] D. von Deak, D. Singh, J.C. King, U.S. Ozkan, Use of carbon monoxide and cyanide to probe the active sites on nitrogen-doped carbon catalysts for oxygen reduction, *Appl. Catal. B-Environ.* 113–114 (2012) 126–133.
- [31] D. von Deak, D. Singh, E.J. Biddinger, J.C. King, B. Bayram, J.T. Miller, U.S. Ozkan, Investigation of sulfur poisoning of CNx oxygen reduction catalysts for PEM fuel cells, *J. Catal.* 285 (2012) 145–151.
- [32] K. Mamanti, D. Jain, D. Zemlyanov, G. Celik, J. Luthman, G. Renkes, A.C. Co, U.S. Ozkan, Probing the oxygen reduction reaction active sites over nitrogen-doped carbon nanostructures (CNx) in acidic media using phosphate anion, *ACS Catal.* 6 (2016) 7249–7259.
- [33] M.R. Rahman, M.I. Awad, F. Kitamura, T. Okajima, T. Ohsaka, A comparative study of ORR at the Pt electrode in ammonium ion-contaminated H<sub>2</sub>SO<sub>4</sub> and HClO<sub>4</sub> solutions, *J. Power Sources* 220 (2012) 65–73.
- [34] Y.-C. Wei, C.-W. Liu, K.-W. Wang, Improvement of oxygen reduction reaction and methanol tolerance characteristics for PdCo electrocatalysts by Au alloying and CO treatment, *R. Soc. Chem. Adv.* 1 (2011) 11927–11929.
- [35] S. Kondo, M. Nakamura, N. Maki, N. Hoshi, Active sites for the oxygen reduction reaction on the low and high index planes of palladium, *J. Phys. Chem. C* 113 (2009) 12625–12628.
- [36] Y. Gorlin, T.F. Jaramillo, A bifunctional nonprecious metal catalyst for oxygen reduction and water oxidation, *J. Am. Chem. Soc.* 132 (2010) 13612–13614.
- [37] J. Duan, S. Chen, M. Jaroniec, S.Z. Qiao, Heteroatom-doped graphene-based materials for energy-relevant electrocatalytic processes, *ACS Catal.* 5 (2015) 5207–5234.
- [38] A. Ajiaz, J. Masa, C. Rosler, W. Xia, P. Weide, A.J. Botz, R.A. Fischer, W. Schuhmann, M. Muhler, Co@Co<sub>3</sub>O<sub>4</sub> encapsulated in carbon nanotube-Grafted nitrogen-Doped carbon polyhedra as an advanced bifunctional oxygen electrode, *Angew. Chem. Int. Ed. Engl.* 55 (2016) 4087–4091.
- [39] J. Masa, W. Xia, I. Sinev, A. Zhao, Z. Sun, S. Grutzke, P. Weide, M. Muhler, W. Schuhmann, Mn(x)O(y)/NC and Co(x)O(y)/NC nanoparticles embedded in a nitrogen-doped carbon matrix for high-performance bifunctional oxygen electrodes, *Angew. Chem. Int. Ed. Engl.* 53 (2014) 8508–8512.
- [40] D. von Deak, E.J. Biddinger, U.S. Ozkan, Carbon corrosion characteristics of CN<sub>x</sub> nanostructures in acidic media and implications for ORR performance, *J. Appl. Electrochem.* 41 (2011) 757–763.
- [41] K.B. Mamanti, D. Jain, A.C. Co, U.S. Ozkan, Nitrogen-coordinated iron-carbon (FeNC) as efficient bifunctional electrocatalysts for oxygen reduction reaction and oxygen evolution reaction in acidic media, *Energy Fuels* 31 (2017) 6541–6547.
- [42] D. Sebastián, A.G. Ruiz, I. Suárez, R. Moliner, M.J. Lázaro, V. Baglio, A. Stassi, A.S. Aricò, Enhanced oxygen reduction activity and durability of Pt catalysts supported on carbon nanofibers, *Appl. Catal. B-Environ.* 115–116 (2012) 269–275.
- [43] X. Wang, W. Li, Z. Chen, M. Waje, Y. Yan, Durability investigation of carbon nanotube as catalyst support for proton exchange membrane fuel cell, *J. Power Sources* 158 (2006) 154–159.
- [44] H.-W. Tien, Y.-L. Huang, S.-Y. Yang, J.-Y. Wang, C.-C.M. Ma, The production of graphene nanosheets decorated with silver nanoparticles for use in transparent, conductive films, *Carbon* 49 (2011) 1550–1560.
- [45] D. Joung, A. Chunder, L. Zhai, S.I. Khondaker, High yield fabrication of chemically reduced graphene oxide field effect transistors by dielectrophoresis, *Nanotechnology* 21 (2010) 165202–165206.
- [46] S.Y. Kim, J. Lee, C.W. Na, J. Park, K. Seo, B. Kim, N-doped double-walled carbon nanotubes synthesized by chemical vapor deposition, *Chem. Phys. Lett.* 413 (2005) 300–305.
- [47] L. Qu, L. Yong, J.-B. Baek, L. Dai, Nitrogen-doped graphene as efficient metal free electrocatalyst for oxygen reduction in fuel cells, *ACS Nano* 4 (2010) 1321–1326.
- [48] J.R. Pels, F. Kapteijn, J.A. Moulijn, Q. Zhu, K.M. Thomas, Evolution of nitrogen functionalities in carbonaceous materials during pyrolysis, *Carbon* 33 (1995) 1641–1653.
- [49] N. Larouche, B.L. Stansfield, Classifying nanostructured carbons using graphitic indices derived from Raman spectra, *Carbon* 48 (2010) 620–629.

- [50] A. Sadezky, H. Muckenhuber, H. Grothe, R. Niessner, U. Pöschl, Raman microspectroscopy of soot and related carbonaceous materials: spectral analysis and structural information, *Carbon* 43 (2005) 1731–1742.
- [51] S. Maldonado, S. Morin, K.J. Stevenson, Structure, composition, and chemical reactivity of carbon nanotubes by selective nitrogen doping, *Carbon* 44 (2006) 1429–1437.
- [52] N.K. Gupta, B. Peng, G.L. Haller, E.E. Ember, J.A. Lercher, Nitrogen modified carbon nano-materials as stable catalysts for phosgene synthesis, *ACS Catal.* 6 (2016) 5843–5855.
- [53] A.N. Buckley, Nitrogen functionality in coals and coal-tar pitch determined by X-ray photoelectron spectroscopy, *Fuel Process. Technol.* 38 (1994) 165–179.
- [54] K. Stanczyk, R. Dziembaj, Z. Piwowarska, S. Witkowski, Transformation of nitrogen structures in carbonization of model compounds determined by XPS, *Carbon* 33 (1995) 1383–1392.